Version of Record: https://www.sciencedirect.com/science/article/pii/S1566119918305160
Manuscript_2715dbd444ac37217cd3e5d037c7b908

Understanding molecular fragmentation in blue phosphorescent organic light-emitting devices

Changyeong Jeong,[a] Caleb Coburn,[b] Muazzam Idris,[c] Yongxi Li,[a] Peter I. Djurovich,[c] Mark E. Thompson,[c] and Stephen R. Forrest[a,b,d,*]

[a)] *Department of Electrical Engineering and Computer Science, University of Michigan, Ann Arbor, MI 48109, USA*

[b)] *Department of Physics, University of Michigan, Ann Arbor, MI 48109, USA*

[c)] *Department of Chemistry, University of Southern California, Los Angeles, CA 90089, USA*

[d)] *Department of Materials Science and Engineering, University of Michigan, Ann Arbor, MI 48109, USA*

** Corresponding author. Telephone: 1-734-647-1147; Fax: 1-734-763-0085; Email: stevefor@umich.edu*

Abstract

We investigate molecular fragmentation in the long lived archetype blue PHOLED guest/host system based on iridium (III) tris[3-(2,6-dimethylphenyl)-7-methylimidazo[1,2-f] phenanthridine] ($Ir(dmp)_3$) and 3,3'-di(9H-carbazol-9-yl)-1,1'-biphenyl (mCBP) as a function of luminance loss using laser desorption ionization time-of-flight mass spectrometry and X-ray photoelectron spectroscopy (XPS). The blue phosphor experiences significant ligand loss due to its labile Ir-ligand bonds, whereas the mCBP host is relatively stable as the luminance decays to 40% of its initial value at 3000 cd/m^2. Density functional theory calculations indicate that fragments from mCBP are less likely to cause luminance loss via exciton quenching compared to those of the Ir-complex. Phosphor fragments are observed by XPS only in aged samples, and the concentration of fragments is found to increase with aging time. These findings suggest that the lifetime of blue PHOLEDs can be improved by using phosphors without labile Ir-ligand and intra-ligand bonds, and a host material that does not form large mass fragments or complexes with the degraded phosphor molecules. Insights into the origin of the loss in luminance due to trap formation from molecular fragmentation of this guest/host system during use are discussed.

© 2018 published by Elsevier. This manuscript is made available under the Elsevier user license
https://www.elsevier.com/open-access/userlicense/1.0/

Introduction

Organic light-emitting devices (OLEDs) are characterized by their low power consumption, aesthetics, and high performance in both pixelated displays and solid-state lighting. Phosphorescent OLEDs (PHOLEDs) have attracted a great deal of attention due to their high efficiency and potentially long device operating lifetimes[1-4]. While red and green PHOLED lifetimes are acceptable for practical use, the relatively short lifetime of blue PHOLEDs remains an impediment to challenge to their implementation[5-12]. Nevertheless, substantial progress has been made in increasing the reliability of blue PHOLEDs based on the archetype iridium (III) tris[3-(2,6-dimethylphenyl)-7-methylimidazo[1,2-f] phenanthridine] ($Ir(dmp)_3$)/3,3'-di(9H-carbazol-9-yl)-1,1'-biphenyl (mCBP) guest/host system[13-16]. While the physical mechanism for efficiency loss over time via nonradiative defect formation by excitonic annihilation events has been established,[13] the chemical origins of these defects has yet to be identified.

In this work, we use a combination of laser desorption ionization time-of-flight mass spectrometry[17-20] (LDI-TOF-MS) and X-ray photoelectron spectroscopy[21-23] (XPS) to investigate molecular fragmentation in both unaged and aged blue PHOLEDs, and are able to infer the molecular degradation pathways that lead to luminance loss over time. Analysis of electrically aged devices show fragmentation of all major constituent molecules, which generally increase in number with device aging time. The most prominent chemical changes are loss of ligand in $Ir(dmp)_3$ and tris-(8-hydroxyquinoline) aluminum (Alq_3), the electron transporting layer (ETL) material, as well as single bond cleavage in the host, mCBP. Notably, we find no evidence for large molecular weight fragments which have been correlated to luminance loss in other luminescent systems[24-26]. Additionally, XPS measurements on UV-irradiated emission layer (EML) films indicate that $Ir(dmp)_3$ undergoes rapid chemical degradation upon irradiation. From

our measurements and density functional theory (DFT) calculations, we infer that fragments from the degraded phosphor are the primary source of traps states that lead to luminance loss.

Results

The PHOLED structure under study and measured energy levels[15-16] are shown in Fig. 1(a). The EML consists of $Ir(dmp)_3$ and mCBP, with the doping concentration of $Ir(dmp)_3$ linearly graded from 18% to 8% from the hole transporting (HTL) to the hole blocking layer (HBL)[14]. Some encapsulated devices were stored in the dark while the remainder were degraded under constant current operation with an initial luminance of L_0 = 3000 cd/m^2 (see Methods). Three samples each were degraded to 80%, 60%, and 40% of their initial brightness (corresponding to T80, T60, and T40, respectively). Figure 1(b) shows the device luminance and voltage rise as functions of aging time. Error bars represent one standard deviation calculated from all device data at the corresponding luminance. Variations in device performance were small, with overall performance similar to previous reports[14].

Figure 1(c) shows mass spectra of the unaged (bottom) and T40 (top) samples, normalized to the mCBP peak intensity. No signal was observed at molecular mass-to-charge ratios greater than that of $Ir(dmp)_3$, $m/z \geq 1198$ amu. All the parent molecules (mCBP, $Ir(dmp)_3$, and Alq_3) and some of their fragments are noted. Low molecular weight mCBP fragments are observed at m/z = 155, 168, and 243 amu (denoted as H1, H2, and H3, respectively), whose logical identities are given in Figure 3. Furthermore, fragments due to loss of the C^N ligand from $Ir(dmp)_3$ are observed at m/z = 334, 526, 668, and 862 amu (D1-D4, respectively), whereas fragments likely due to rupture of pendent xylyl and methyl groups on the ligands are at m/z = 1093 and 1181 amu (D6 and D7, respectively, see Supplementary Fig. 1). Fragments observed at m/z = 927 amu are consistent with loss of xylene and two carbons on the imidazole heterocyclic

portion of two ligands, as well as loss of a methyl group (D5, see Supplementary Fig. 1). The intensities of these fragment peaks do not change with degradation time, indicating that they are generated during the LDI-TOF-MS measurement. Alq_3 shows fragment peaks at *m/z* = 143, 173, 316, and 773 amu (E1-E4, respectively, see Supplementary Fig. 2), where E3 and E4 are independent of degradation time. We note that several of the molecular fragments are produced during the LDI-TOF-MS measurement. These measurement-induced fragments are observed in the unaged device mass spectrum, and hence are taken into account in our aging analysis.

We tracked the relative intensities of $Ir(dmp)_3$ and mCBP fragment peaks compared to undegraded mCBP as a function of luminance loss, with results shown in Figs. 2(a) and (b), respectively. Error bars are the standard deviations of the intensity data of three samples. All fragments are present in the mass spectra of the unaged samples, but their increase in peak height with time indicates that the molecules undergo further fragmentation during aging. Some peaks do not change with luminance loss, suggesting that the corresponding fragments do not form during device operation.

Figures 3(a) and (b) show fragmentation products of $Ir(dmp)_3$ and mCBP, respectively. The $Ir(dmp)_3$ molecular fragments are generated by dissociation of Ir bonds to the coordinated N and C atoms. $Ir(dmp)_3$ is dissociated into D1 and D4 by ligand loss, and into D2 by loss of a second ligand. The fragment D3 corresponds to two dissociated dmp ligands that are coupled together, presumably formed by reductive elimination of the two ligands. The loss of xylyl and methyl groups to form D6 and D7, respectively, are shown in Supplementary Fig. 1. The peak intensities of D6 and D7, shown in Fig. 1(c), are approximately 30 and 10 times lower, respectively, than those of the $Ir(dmp)_3$ fragment peaks created by loss of the C^N ligand. The mCBP fragments are generated by cleavage of the single C-N and C-C bond to and within the

biphenyl core, respectively. Rupture of the C-N bond results in carbazole (H2) and biphenylcarbazole (H4). However, the signal for biphenylcarbazole is hidden in the mass spectra by the large Alq_3 fragment and associated isotope peaks. Bond rupture of C-N in biphenylcarbazole generates biphenyl (H1) and carbazole, and C-C bond cleavage results in phenylcarbazole (H3), producing the protonated fragments for H1 and H3. Also, Alq_3 dissociates by ligand loss, as reported previously[17, 27]. Additionally, we measured LDI-TOF-MS for unaged films of bis(2-(4,6-difluorophenyl)pyridyl-N,C2')iridium(III)picolinate (FIrpic), iridium(III)bis(2,4-difluorophenylpyridinato)tetrakis(1-pyrazolyl)borate (FIr6), tris[1-(2,6-diisopropylphenyl)-2-phenyl-1H-imidazole]iridium(III) ($Ir(iprpmi)_3$), and a Pt complex with carbazolyl-pyridine cyclometalating ligands (PtNON), with results given in Supplementary Figs. 5-1 and 5-2. For FIrpic and FIr6, we observe intense fragment peaks with little or no parent molecular peak intensity. In contrast, PtNON and $Ir(iprpmi)_3$ exhibit intense molecular peaks but relatively small fragment signals.

Figure 4 shows an energy level diagram of the EML with the frontier orbital energies of each fragment calculated via DFT. Triplet energies calculated by TD-DFT are also given. The neutral, radical, cation, and anion forms of the fragments are illustrated in cyan, orange, green, and violet, respectively. Fragment energies omitted in Fig. 4 could not be solved by DFT. The calculated highest occupied molecular orbital (HOMO) and lowest unoccupied molecular orbital (LUMO) energies for mCBP and $Ir(dmp)_3$ in Fig. 4 agree with the measured values in Fig 1(a).

Figure 5 shows XPS data for EML films aged under 162.0 mW/cm^2, 365 nm wavelength illumination (See Methods). Figure 5(a) shows the Ir 4f XPS spectra for unaged and aged films along with Gaussian fits to the T40 data. Peaks at 61.3 eV and 64.3 eV correspond to Ir $4f_{7/2}$ and Ir $4f_{5/2}$, respectively. The unaged sample shows two $Ir(dmp)_3$ peaks, while the aged samples

show two additional fragment peaks. The full-width half maximum of the fragment peaks obtained is *FWHM* = 2.26±0.11 eV, while for $Ir(dmp)_3$, *FWHM* = 0.73±0.01 eV. Fragment peak energies are shifted to 62.15±0.07 eV and 65.27±0.11 eV, respectively. Figure 5(b) shows the intensity change of $Ir(dmp)_3$, and the ratio of the fragment to that of $Ir(dmp)_3$ (i.e. Frag/$Ir(dmp)_3$) vs. luminance loss. Frag/$Ir(dmp)_3$ intensities gradually increase while the $Ir(dmp)_3$ peaks decrease. Figure 5(c) shows the N 1s XPS spectra of the unaged and aged films. Corresponding measurements for neat films of unaged mCBP and $Ir(dmp)_3$ are given in Supplementary Fig. 3. The prominent peak at 400.7 eV corresponds primarily to mCBP, with a small overlapping contribution from the $Ir(dmp)_3$ peak at 401.2 eV. The small peak observed at 399.3 eV also results from $Ir(dmp)_3$. The $Ir(dmp)_3$ peak at 399.3 decreases by 38% at T80, whereas the mCBP peak is almost unchanged over the same time. Unlike the Ir 4f spectra, no new N 1s peak is observed after aging.

Discussion

Previous LDI-TOF-MS investigations of aged OLEDs focused primarily on fragment peaks that are present only in the aged device spectra.[27-33] However, it is likely that fragments formed during electrical operation are also formed when molecules are ablated during the LDI-TOF-MS measurement. Therefore, in Fig. 2 each fragment peak is plotted as a function of luminance loss to identify fragments created during electrical operation. The fragment peaks are normalized with mCBP since the presence of degradation-independent fragment peaks after normalization to mCBP, the small magnitude of mCBP fragment peaks, and small intensity change of mCBP as measured by XPS indicate that mCBP is unlikely to be significantly degraded during device operation relative to the other molecules.

The D1-D4 fragments generated from loss of ligands show relatively large peak heights, whereas D6 and D7 generated from loss of pendent groups on the ligands are lower in intensity. This difference suggests that $Ir(dmp)_3$ degrades by two separate pathways during device operation. Blue emissive cyclometalated Ir phosphors have high triplet state energies. Cleavage of the Ir-N bond is proposed to occur in these complexes by thermal activation from the triplet excited state to form an unstable, five-coordinated intermediate species[34-36]. Subsequent breaking of the Ir-C bond in this intermediate will lead to loss of the ligand. Loss of the pendent methyl and aryl groups are likely due to homolytic cleavage of the ligand-methyl/aryl C-C bond. The C-C bond dissociation energy is large (*BDE* = 4.41-4.97 eV, see Supplementary Fig. 4) and greater than the BDE of the Ir-C bond, which is estimated to be 3.45 eV for a $Ir\text{-}C_6H_5$ bond[37]. The relatively low BDE of the Ir-C bond will thus favor loss of the ligand from the five-coordinated intermediate over rupture of the pendent groups on the ligand.

The energy levels of the degraded fragments are important to consider, since fragments with low triplet energies (E_T) can be sites for exciton quenching. Also, fragments with a LUMO < - 1.5 eV or HOMO > - 4.8 eV below the vacuum level lie within the energy gap of the molecular species, leading to Shockley-Read-Hall non-radiative recombination and exciton quenching[13]. According to DFT calculations shown in Fig. 4, the D6, H1, H3, and H4 radicals have deeper LUMOs than mCBP, suggesting that the radical species generated during operation can trap electrons, forming recombination centers that likely lead to a drop in luminescence and an increase in voltage according to the theory in Ref. 13. In principle, these radical fragments can react with other molecules to form a molecule of higher mass, although this was not observed. The D7 radical can quench exciton since it has lower E_T than $Ir(dmp)_3$. This fragment species, however, does not have an impact on charge trapping due its wide energy gap. Further, mCBP

forms neutral fragments (i.e. carbazole, phenyl-carbazole, etc.) upon proton abstraction. These have wider energy gaps and higher E_T than $Ir(dmp)_3$, and hence they, too, are inactive in the aging process.

Figure 4 shows that the D2, D4, and H1-H4 cations have deeper LUMO energies than the HOMO of the dopant. These positively charged fragments can attract electrons to become neutral species as shown, and hence do not persist as electronically active states. This leaves the anion series of D1 and H1-H4. Electron transfer from these states will also be rapid, converting them to neutral species. Thus, only the neutral fragments, D6, H1, H3, and H4, appear to be responsible for the non-radiative recombination leading to luminance loss and voltage rise over time.[13,16] Also, the DFT calculation shows that these species have lower E_T than $Ir(dmp)_3$, suggesting that they are likely to be sources of exciton quenching that is not included in the TPA model of Ref. 13.

The stability of mCBP and relatively benign nature of its degradation products make it a suitable host/blocking material that resists complexation with $Ir(dmp)_3$ and Alq_3 fragments, as well as complexation with its own fragments. We also observe no large-mass $Ir(dmp)_3$-Alq_3 fragment compounds, which have previously been attributed to luminance loss[24, 26, 29-30, 32]. We conclude that both characteristics are key to phosphor stability: the host and blocking materials should not lead to deleterious fragments upon degradation and should not be vulnerable to complexation with the degraded phosphor molecular fragments.

To further understand the stability of $Ir(dmp)_3$, we used LDI-TOF-MS to compare fragmentation of four additional blue-emitting phosphors. FIrpic and FIr6, which result in relatively short-lived PHOLEDs compared with $Ir(dmp)_3$[31], show fragments due to loss of ligand loss in their mass spectra and have insignificant signal intensities for the parent molecules

themselves. In contrast, $Ir(dmp)_3$, $Ir(iprpmi)_3$, and PtNON give relatively long-lived PHOLEDs[14, 16, 38-39] and show peaks of largest intensity at their parent molecular weights in the mass spectra. Supplementary Fig. 5-1(a) shows that the fragment generated from the loss of the picolinate (N^O) ligand has the highest intensity, whereas no fragment peak due to loss of the cyclometalated (N^C) ligand is observed, suggesting that picolinate is more labile than the cyclometalated ligand. For FIr6, the dominant fragment peaks result from loss of the tetrakispyrazolyl borate (N^N) ligand and B-N bond cleavage, demonstrating that N^N ligand is more labile than the C^N ligand. The difference in fragmentation products suggests that the N^O and N^N ligands are bound less strongly to iridium than the N^C ligands. The stable dopants $Ir(iprpmi)_3$ and $Ir(dmp)_3$ have only Ir-(N^C) bonds, and do not show noticeably large peaks for fragmentation in their mass spectra, compared to the signal intensity for the parent molecular ion. Finally, the largest signals in the mass spectrum of PtNON comes from the parent structure, along with a relatively large fragment peak due to loss of Pt from the complex. From these several observations, we infer that the stability of the Ir-ligand bond in a phosphor is strongly correlated with its stability in PHOLEDs, and phosphors with Ir-(N^C) bonds such as $Ir(dmp)_3$ can lead to higher stability than phosphors (e.g. FIr6 and FIrpic) with Ir-(N^O) and Ir-(N^N) bonds in a device.

The new peaks in the Ir 4f XPS measurements of the aged EML films indicate the generation of $Ir(dmp)_3$ fragments and confirm that the dopant is chemically altered after prolonged UV irradiation. The relatively large *FWHM* of the fragment peaks compared to $Ir(dmp)_3$ shown in Fig. 5(a) likely result from multiple overlapping fragment signals, which are consistent with the data from LDI-TOF-MS analysis. Additionally, the trend of decreasing $Ir(dmp)_3$ and increasing fragment Ir 4f peaks with time shown in Fig. 5(b) are consistent with the

formation of molecular and fragment peaks observed in the LDI-TOF-MS measurements. The absence of new peaks after aging in Fig. 5(c) may be due to a low density of fragments, or fragments with N 1s binding energies that are degenerate with mCBP. The similar mCBP peak heights and the change in the peak intensity ratio with aging support the conclusion that $Ir(dmp)_3$ degrades upon irradiation, suggesting that mCBP does not experience significant degradation due to bimolecular annihilation process occurring in $Ir(dmp)_3$. Faster degradation of $Ir(dmp)_3$ compared with mCBP under UV radiation indicates that bond strength and/or exciton localization determines the relative degradation rates, rather than damage due to charge transport by a particular molecule.

Intrinsic degradation in blue PHOLEDs has been attributed to energy released by hot excited states generated from bimolecular annihilation. Different studies have concluded that triplet-triplet annihilation (TTA) or triplet-polaron annihilation (TPA) result in the hot excited states[13-14, 16, 40-41]. The preponderance of evidence supports TPA as the dominant mechanism leading to luminance loss arising from electrical excitation.[13-14, 40] In the present study, however, fragmentation was observed upon UV irradiation in the absence of current, indicating that other mechanisms are also active, such as unimolecular degradation of the exciton or TTA.

Intrinsic luminance loss due to molecular fragmentation in the EML occurs through trap-assisted recombination and quenching of excitons at low E_T fragments[13]. While it is possible that some fragments form shallow traps with high E_T, these types of degradation products likely do not contribute to luminance loss, as opposed to fragments with E_T lower than that of $Ir(dmp)_3$ and/or mid-energy gap transport levels. DFT calculations indicate several of the fragments identified in this work have energy levels that are likely to cause luminance loss via these energy/electron transfer mechanisms. We also note that additional red emission has been

observed in degraded FIr6 devices[31]. However, we observe no spectral change with degradation other than reduced intensity from $Ir(dmp)_3$, indicating that products formed upon degradation are not luminescent. Finally, both XPS and LDI-TOF-MS measurements indicate that only a small fraction of $Ir(dmp)_3$ dopants fragment, even at > 50% luminance loss. This result supports the conclusion that luminance loss is due to quenching and trap-assisted recombination rather than the depletion of viable dopant molecules.

Conclusion

We investigated molecular fragmentation of archetype, long-lived blue PHOLEDs. We found that the phosphor dissociates by loss of ligand, as well as rupture of substituents on the ligand, with the former process being the dominant fragmentation pathway. DFT calculations indicate that fragments from mCBP are less likely to trap charges and quench excitons than those of the phosphor. Additionally, we do not observe formation of high mass compounds during degradation, which are more likely to form deep traps. XPS and LDI-TOF-MS results consistently indicate that the $Ir(dmp)_3$ fragment concentration increases with time. The XPS data show that the $Ir(dmp)_3$ fragments appear at noticeably higher binding energies with a wider *FWHM* than $Ir(dmp)_3$, whereas the N 1s spectra in the aged and unaged samples are not significantly different, consistent with our conclusion that $Ir(dmp)_3$ degradation is primarily responsible for the luminance loss. Comparing this work with previous LDI-TOF-MS studies on blue emitting phosphor compounds, we conclude that materials in short wavelength emitting PHOLEDs should be selected to avoid complexation of fragments, and primarily based on phosphor compounds having strong bonds of metal-ligand and pendent groups in ligands.

Acknowledgements

This work was supported by the United States Department of Energy under award DE-EE0007077, Universal Display Corporation, and the Air Force Office of Scientific Research under Award No. FA9550-14-1-0245. The authors are grateful for technical support from the Michigan Center for Materials Characterization. The authors thank Drs. Jim Windak, Tyler Fleetham, Shaocong Hou, and Mr. Kan Ding and Yue Qu for valuable discussions.

Methods:

Sample Preparation: The device structure used for LDI-TOF-MS is: 1.1 mm thick glass substrate/150 nm indium tin oxide (ITO)/10 nm dipyrazino[2,3,-f:20,30-h]quinoxaline2,3,6,7,10,11-hexacarbonitrile (HATCN)/50 nm mCBP:18→8 vol% $Ir(dmp)_3$ / 5 nm mCBP/30 nm Alq_3/1.5 nm 8-hydroxyquinolinato lithium (Liq) /100 nm Al. XPS films have the following structure: 1.1 mm thick glass/30 nm mCBP:13 vol% $Ir(dmp)_3$. HATCN, mCBP. The $Ir(dmp)_3$ was provided by Universal Display Corporation (UDC) and used as received. Alq_3 was purchased from Sigma-Aldrich and purified by thermal gradient sublimation[42]. Devices were encapsulated under a nitrogen environment in a glovebox with $\leq$ 0.1 ppm H_2O and O_2 using a cover glass with a UV-cured epoxy seal around the periphery. The substrates were cleaned in tergitol and deionized water for 10 min, and by acetone and isopropanol for 30 min. The substrates were then snow-cleaned for 20 s and exposed by UV ozone for 30 min immediately prior to film growth. All films were deposited by thermal evaporation at deposition rates between 0.1-1 Å/s and a base pressure $\leq 3 \times 10^{-7}$ Torr.

LDI-TOF-MS: After aging, the cover glass was removed and the Al cathode covering the active area was carefully peeled off using scotch tape[33], followed by mounting the samples onto the LDI-TOF-MS target plate. Bruker LDI-TOF-MS Autoflex Speed with Smartbeam II was used in the reflection mode for high mass resolution. The wavelength, pulse width, laser energy, source acceleration voltage, and the detector gain voltage were 355 nm, 10 ns, 275 μJ, 19 kV, and 2071 V, respectively. The mass spectra between 100 and 2000 *m/z* for each device were obtained for ten spots. The masses were calibrated with the mCBP peak at *m/z* = 484. Each spot was measured for 100 laser pulses at 25 Hz and at $\leq 3 \times 10^{-7}$ Torr. Each peak intensity considered is 10 times greater than the standard deviation of the background noise. No noticeable signal was observed for LDI-TOF-MS on a bare ITO substrate. Large area (21 mm^2) devices were fabricated to ensure that the 10 measured spots do not overlap to prevent sample changes due to the repetitive measurement from the laser desorption process. Fragments were identified based on molecular weight and isotopic distribution (See Supplementary Fig. 6).

XPS: Samples were degraded by the high power UV-LED projector at a center wavelength of 365 nm and a 20 nm FWHM. Unaged samples were encapsulated and stored in the dark. T80 and T60 samples were stored in dark after aging without removing the cover glasses until the T40 samples were fully degraded. The films were then loaded into the XPS chamber, requiring < 1 min exposure to ambient air. The monochromatized Al *Kα* source (1486.6 eV) was excited at 10 mA and 12 kV, and the spectrum was calibrated to the Au($4f_{7/2}$) peak, 84.0 eV. All spectra for both N 1s and Ir 4f were measured at $< 3 \times 10^{-9}$ Torr and averaged over 75 scans. The spectra show slightly decreased intensities after aging, likely due to exposure from trace amounts of O_2 and H_2O trapped within the encapsulation.

DFT and TD-DFT Calculations: Calculations were performed using Jaguar version 9.8 (release 11) software package on the Schrödinger Material Science Suite (v2017-4). DFT was used to optimize the orbital geometries while TD-DFT was used to calculate orbital contribution for singlet transitions. The gas phase geometry optimization was calculated using the B3LYP functional with the LACVP** basis set. The HOMO and LUMO energies were determined using minimized singlet geometries to approximate the ground state, whereas the optimized triplet geometries were used to approximate the triplet excited state. *BDE*s were calculated using the B3LYP functional and LACV3P** basis set.

References

1. Baldo, M. A.; O'Brien, D. F.; You, Y.; Shoustikov, A.; Sibley, S.; Thompson, M. E.; Forrest, S. R., Highly efficient phosphorescent emission from organic electroluminescent devices. *Nature* **1998,** *395* (6698), 151-154.

2. Baldo, M. A.; Lamansky, S.; Burrows, P. E.; Thompson, M. E.; Forrest, S. R., Very high-efficiency green organic light-emitting devices based on electrophosphorescence. *Applied Physics Letters* **1999,** *75* (1), 4-6.

3. Adachi, C.; Baldo, M. A.; Forrest, S. R.; Thompson, M. E., High-efficiency organic electrophosphorescent devices with tris(2-phenylpyridine)iridium doped into electron-transporting materials. *Applied Physics Letters* **2000,** *77* (6), 904-906.

4. Baldo, M. A.; Thompson, M. E.; Forrest, S. R., High-efficiency fluorescent organic light-emitting devices using a phosphorescent sensitizer. *Nature* **2000,** *403* (6771), 750-3.

5. Chwang, A. B.; Kwong, R. C.; Brown, J. J., Graded mixed-layer organic light-emitting devices. *Applied Physics Letters* **2002,** *80* (5), 725-727.

6. Kwong, R. C.; Nugent, M. R.; Michalski, L.; Ngo, T.; Rajan, K.; Tung, Y.-J.; Weaver, M. S.; Zhou, T. X.; Hack, M.; Thompson, M. E.; Forrest, S. R.; Brown, J. J., High operational stability of electrophosphorescent devices. *Applied Physics Letters* **2002,** *81* (1), 162-164.

7. Kwong, R. C.; Weaver, M. S.; Michael Lu, M.-H.; Tung, Y.-J.; Chwang, A. B.; Zhou, T. X.; Hack, M.; Brown, J. J., Current status of electrophosphorescent device stability. *Organic Electronics* **2003,** *4* (2-3), 155-164.

8. Meerheim, R.; Walzer, K.; Pfeiffer, M.; Leo, K., Ultrastable and efficient red organic light emitting diodes with doped transport layers. *Applied Physics Letters* **2006,** *89* (6), 061111.

9. Kondakova, M. E.; Pawlik, T. D.; Young, R. H.; Giesen, D. J.; Kondakov, D. Y.; Brown, C. T.; Deaton, J. C.; Lenhard, J. R.; Klubek, K. P., High-efficiency, low-voltage phosphorescent organic light-emitting diode devices with mixed host. *Journal of Applied Physics* **2008,** *104* (9), 094501.

10. Fleetham, T.; Li, G.; Li, J., Efficient Red-Emitting Platinum Complex with Long Operational Stability. *ACS Appl Mater Interfaces* **2015,** *7* (30), 16240-6.

11. Lee, J. H.; Shin, H.; Kim, J. M.; Kim, K. H.; Kim, J. J., Exciplex-Forming Co-Host-Based Red Phosphorescent Organic Light-Emitting Diodes with Long Operational Stability and High Efficiency. *ACS Appl Mater Interfaces* **2017,** *9* (4), 3277-3281.

12. Zhu, Z. Q.; Klimes, K.; Holloway, S.; Li, J., Efficient Cyclometalated Platinum(II) Complex with Superior Operational Stability. *Adv Mater* **2017,** *29* (6).

13. Giebink, N. C.; D'Andrade, B. W.; Weaver, M. S.; Mackenzie, P. B.; Brown, J. J.; Thompson, M. E.; Forrest, S. R., Intrinsic luminance loss in phosphorescent small-molecule organic light emitting devices due to bimolecular annihilation reactions. *Journal of Applied Physics* **2008,** *103* (4), 044509-044512.

14. Zhang, Y. F.; Lee, J.; Forrest, S. R., Tenfold increase in the lifetime of blue phosphorescent organic light-emitting diodes. *Nature Communications* **2014,** *5*, 5008-5015.

15. Coburn, C.; Lee, J.; Forrest, S. R., Charge Balance and Exciton Confinement in Phosphorescent Organic Light Emitting Diodes. *Advanced Optical Materials* **2016,** *4* (6), 889-895.

16. Lee, J.; Jeong, C.; Batagoda, T.; Coburn, C.; Thompson, M. E.; Forrest, S. R., Hot excited state management for long-lived blue phosphorescent organic light-emitting diodes. *Nature Communications* **2017,** *8*.

17. Scholz, S.; Corten, C.; Walzer, K.; Kuckling, D.; Leo, K., Photochemical reactions in organic semiconductor thin films. *Organic Electronics* **2007,** *8* (6), 709-717.

18. Duncan, M. W.; Roder, H.; Hunsucker, S. W., Quantitative matrix-assisted laser desorption/ionization mass spectrometry. *Brief Funct Genomic Proteomic* **2008,** *7* (5), 355-70.

19. Damnjanović, B.; Kamčeva, T.; Petrović, B.; Bugarčić, Ž. D.; Petković, M., Laser desorption and ionization time-of-flightversus matrix-assisted laser desorption and ionization time-of-flight mass spectrometry of Pt(ii) and Ru(iii) metal complexes. *Anal. Methods* **2011,** *3* (2), 400-407.

20. Huang, L.; Wan, J.; Wei, X.; Liu, Y.; Huang, J.; Sun, X.; Zhang, R.; Gurav, D. D.; Vedarethinam, V.; Li, Y.; Chen, R.; Qian, K., Plasmonic silver nanoshells for drug and metabolite detection. *Nat Commun* **2017,** *8* (1), 220.

21. Le, Q. T.; Avendano, F. M.; Forsythe, E. W.; Yan, L.; Gao, Y.; Tang, C. W., X-ray photoelectron spectroscopy and atomic force microscopy investigation of stability mechanism of

tris-(8-hydroxyquinoline) aluminum-based light-emitting devices. *Journal of Vacuum Science & Technology A: Vacuum, Surfaces, and Films* **1999,** *17* (4), 2314-2317.

22. Choo, D. C.; Kim, T. W., Degradation mechanisms of silver nanowire electrodes under ultraviolet irradiation and heat treatment. *Sci Rep* **2017,** *7* (1), 1696.

23. Freakley, S. J.; Ruiz-Esquius, J.; Morgan, D. J., The X-ray photoelectron spectra of Ir, IrO2

and IrCl3

revisited. *Surface and Interface Analysis* **2017,** *49* (8), 794-799.

24. Scholz, S.; Meerheim, R.; Lüssem, B.; Leo, K., Laser desorption/ionization time-of-flight mass spectrometry: A predictive tool for the lifetime of organic light emitting devices. *Applied Physics Letters* **2009,** *94* (4), 043314.

25. de Moraes, I. R.; Scholz, S.; Lüssem, B.; Leo, K., Chemical degradation processes of highly stable red phosphorescent organic light emitting diodes. *Organic Electronics* **2012,** *13* (10), 1900-1907.

26. de Moraes, I. R.; Scholz, S.; Leo, K., Influence of the applied charge on the electro-chemical degradation in green phosphorescent organic light emitting diodes. *Organic Electronics* **2016,** *38*, 164-171.

27. Scholz, S.; Lüssem, B.; Leo, K., Chemical changes on the green emitter tris(8-hydroxy-quinolinato)aluminum during device aging of p-i-n-structured organic light emitting diodes. *Applied Physics Letters* **2009,** *95* (18), 183309.

28. Sivasubramaniam, V.; Brodkorb, F.; Hanning, S.; Buttler, O.; Loebl, H. P.; van Elsbergen, V.; Boerner, H.; Scherf, U.; Kreyenschmidt, M., Degradation of HTL layers during device operation in PhOLEDs. *Solid State Sciences* **2009,** *11* (11), 1933-1940.

29. Moraes, I. R. d.; Scholz, S.; Lüssem, B.; Leo, K., Analysis of chemical degradation mechanism within sky blue phosphorescent organic light emitting diodes by laser-desorption/ionization time-of-flight mass spectrometry. *Organic Electronics* **2011,** *12* (2), 341-347.

30. de Moraes, I. R.; Scholz, S.; Lüssem, B.; Leo, K., Role of oxygen-bonds in the degradation process of phosphorescent organic light emitting diodes. *Applied Physics Letters* **2011,** *99* (5), 053302.

31. Seifert, R.; Rabelo de Moraes, I.; Scholz, S.; Gather, M. C.; Lüssem, B.; Leo, K., Chemical degradation mechanisms of highly efficient blue phosphorescent emitters used for organic light emitting diodes. *Organic Electronics* **2013,** *14* (1), 115-123.

32. Wölzl, F.; Rabelo de Moraes, I.; Lüssem, B.; Hofmann, S.; Leo, K.; Gather, M. C., Performance and lifetime of vacuum deposited organic light-emitting diodes: Influence of residual gases present during device fabrication. *Organic Electronics* **2014,** *15* (11), 3251-3258.

33. Dong, S.-C.; Xu, L.; Tang, C. W., Chemical degradation mechanism of TAPC as hole transport layer in blue phosphorescent OLED. *Organic Electronics* **2017,** *42*, 379-386.

34. Sajoto, T.; Djurovich, P. I.; Tamayo, A. B.; Oxgaard, J.; Goddard, W. A.; Thompson, M. E., Temperature Dependence of Blue Phosphorescent Cyclometalated Ir(III) Complexes. *Journal of the American Chemical Society* **2009,** *131* (28), 9813-9822.

35. Treboux, G.; Mizukami, J.; Yabe, M.; Nakamura, S., Blue phosphorescent Iridium(III) complex. A reaction path on the triplet potential energy surface. *Chemistry Letters* **2007,** *36* (11), 1344-1345.

36. Zhou, X. W.; Burn, P. L.; Powell, B. J., Bond Fission and Non-Radiative Decay in Iridium(III) Complexes. *Inorganic Chemistry* **2016,** *55* (11), 5266-5273.

37. Nolan, S. P.; Hoff, C. D.; Stoutland, P. O.; Newman, L. J.; Buchanan, J. M.; Bergman, R. G.; Yang, G. K.; Peters, K. S., Heats of Reaction of Cp-Star(Pme3)Ir(C6h5)(H), Cp-Star(Pme3)Ir(C6h11)(H), Cp-Star(Pme3)Ir(H)(H) with Hcl, Ccl4, Cbr4, and Ch3i - a Solution Thermochemical Study of the C-H Insertion Reaction. *Journal of the American Chemical Society* **1987,** *109* (10), 3143-3145.

38. Klubek, K. P.; Dong, S.-C.; Liao, L.-S.; Tang, C. W.; Rothberg, L. J., Investigating blue phosphorescent iridium cyclometalated dopant with phenyl-imidazole ligands. *Organic Electronics* **2014,** *15* (11), 3127-3136.

39. Fleetham, T. B.; Huang, L.; Klimes, K.; Brooks, J.; Li, J., Tetradentate Pt(II) Complexes with 6-Membered Chelate Rings: A New Route for Stable and Efficient Blue Organic Light Emitting Diodes. *Chemistry of Materials* **2016,** *28* (10), 3276-3282.

40. Giebink, N. C.; D'Andrade, B. W.; Weaver, M. S.; Brown, J. J.; Forrest, S. R., Direct evidence for degradation of polaron excited states in organic light emitting diodes. *Journal of Applied Physics* **2009,** *105* (12).

41. Wang, Q.; Sun, B.; Aziz, H., Exciton-Polaron-Induced Aggregation of Wide-Bandgap Materials and its Implication on the Electroluminescence Stability of Phosphorescent Organic Light-Emitting Devices. *Advanced Functional Materials* **2014,** *24* (20), 2975-2985.

42. Mcghie, A. R.; Garito, A. F.; Heeger, A. J., Gradient Sublimer for Purification and Crystal-Growth of Organic Donor and Acceptor Molecules. *Journal of Crystal Growth* **1974,** *22* (4), 295-297.

Figure Captions

Figure 1: Device lifetimes and mass spectra. (a) Blue phosphorescent device structure and proposed energy diagram, including layer thicknesses and materials. The emission layer (EML) consists of mCBP linearly doped from 18% to 8% with $Ir(dmp)_3$ from the HATCN to the mCBP layer interfaces. Numbers correspond to highest occupied (HOMO) and lowest unoccupied molecular orbital (LUMO) energies denoted from the vacuum level. **(b)** Luminance loss and voltage rise vs. time, with initial luminance of L_0 = 3000 cd/m^2. The data represent nine samples, with three each removed from life-testing at T80, T60, and T40, respectively. Color breaks indicate times when samples were removed, and the error bars represent one standard deviation of the samples on test. **(c)** Mass spectra of the unaged (bottom) and T40 (top) aged samples. Parent and fragment molecules are labelled in violet and blue, respectively. The mass spectra are normalized and calibrated with mCBP. No signal was observed at *m/z* = 1200 – 2000.

Figure 2: Fragment generation in emission layers with luminance loss. (a) $Ir(dmp)_3$ and its major fragments as a function of the luminance loss. Only fragments that are generated during electrical operation are displayed. **(b)** mCBP and its fragments as a function of the luminance loss. The error bars represent one standard deviation from three samples.

Figure 3: Molecular fragmentation products. (a) Molecular fragmentation products proposed for $Ir(dmp)_3$. $Ir(dmp)_3$ is dissociated into the fragments with *m/z* = 334 and 862 illustrated in red (D1) and black (D4), respectively, and then further dissociated into the *m/z* = 526 (D2) by ligand loss. Dissociated $Ir(dmp)_3$ ligands are combined to form the fragment with *m/z* = 668 (D3). **(b)** Proposed fragmentation products of mCBP. C-N bond cleavage can generate biphenyl, carbazole, and biphenylcarbazole (H1, H2, and H4, respectively). The C-C bond cleavage generates phenylcarbazole (H3).

Figure 4: Energy level diagram of the fragments produced on PHOLED aging. The LUMO energy of mCBP and the HOMO energy of $Ir(dmp)_3$ are illustrated by the shaded region. Anion, cation, radical, and neutral species are displayed in violet, green, orange, and cyan, respectively. Triplet energies of the parent as well as neutral and radical fragment molecules are given at the bottom right. Omitted values do not converge in the DFT calculation.

Figure 5: X-ray photoelectron spectroscopy spectra tracking device aging. (a) Ir 4f XPS spectra of the unaged and aged samples. The aged spectra show new peaks at 62.15±0.07 eV and 65.27±0.11 eV due to fragmentation. The T40 data are fit to a Gaussian function and displayed with solid lines for the $Ir(dmp)_3$ and fragment signals. **(b)** Intensity changes of $Ir(dmp)_3$ and the fragment/$Ir(dmp)_3$ intensity ratio (Frag/$Ir(dmp)_3$) as a function of luminance loss. The fragment peak intensity increases with aging while the $Ir(dmp)_3$ peak decreases. The error bars represent 95% confidence intervals for the fits. **(c)** N 1s XPS spectra of the unaged and aged samples. The $Ir(dmp)_3$ peak at 399.3 eV shows noticeable reduction at T80, while mCBP does not.

Figure 1

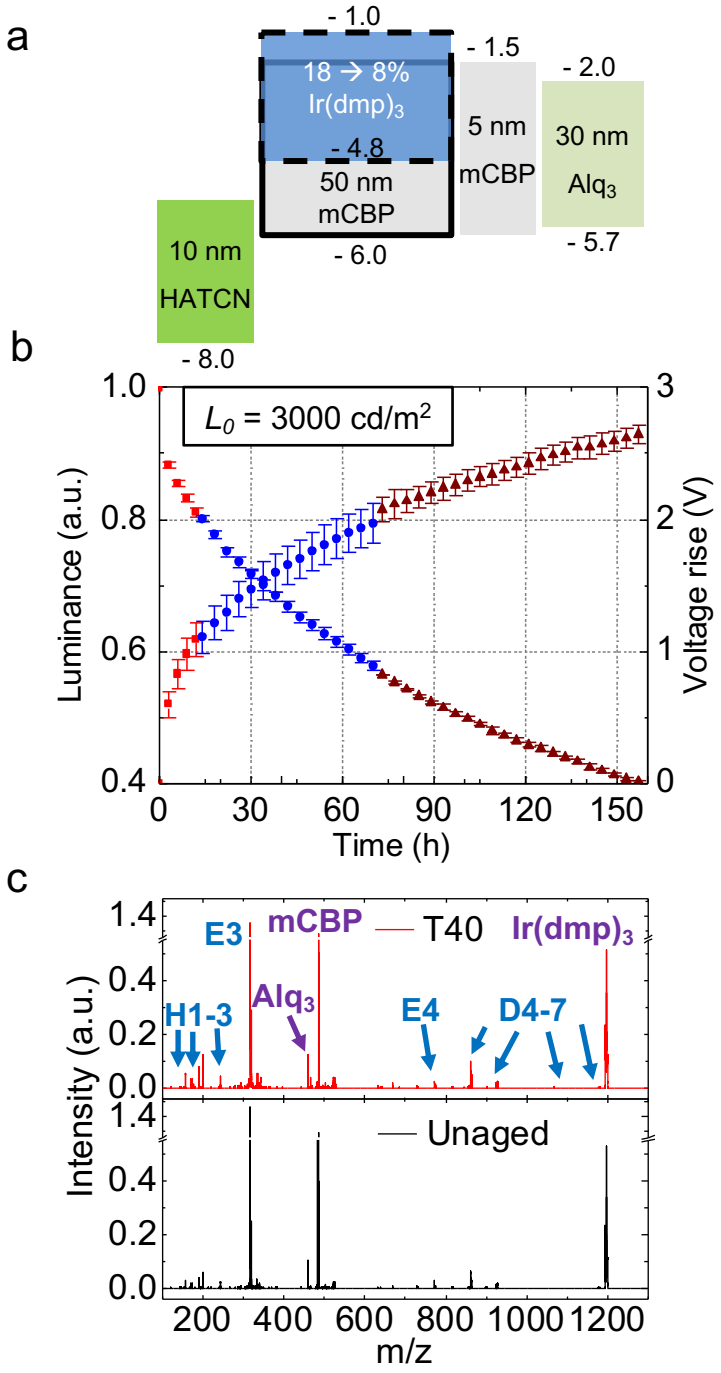
a
- 1.0
18 → 8%
Ir(dmp)3
- 4.8
50 nm
mCBP
- 1.5
5 nm
mCBP
- 2.0
30 nm
Alq3
- 5.7
10 nm
HATCN
- 8.0
b
L0 = 3000 cd/m2
Luminance (a.u.)
Voltage rise (V)
Time (h)
c
E3
mCBP
T40
Ir(dmp)3
H1-3
Alq3
E4
D4-7
Unaged
Intensity (a.u.)
m/z

Figure 2

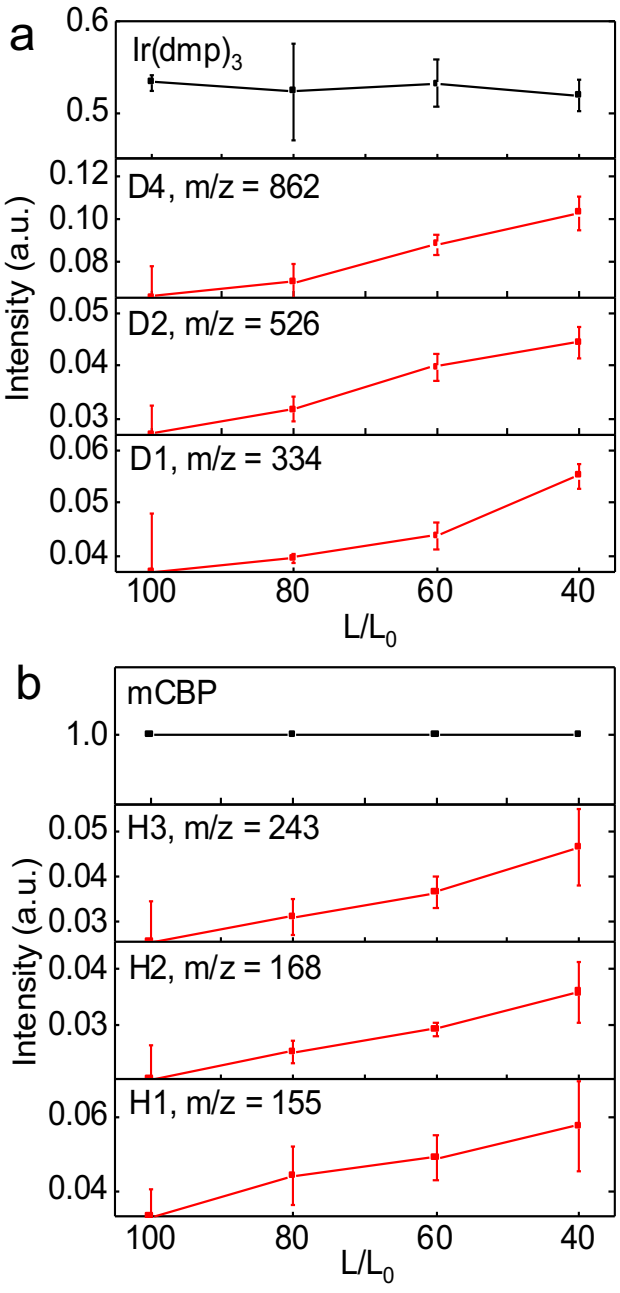
a
Ir(dmp)3
0.6
0.5
D4, m/z = 862
0.12
0.10
0.08
D2, m/z = 526
0.05
0.04
0.03
D1, m/z = 334
0.06
0.05
0.04
Intensity (a.u.)
100
80
60
40
L/L0
b
mCBP
1.0
H3, m/z = 243
0.05
0.04
0.03
H2, m/z = 168
0.04
0.03
H1, m/z = 155
0.06
0.04
Intensity (a.u.)
100
80
60
40
L/L0

Figure 3

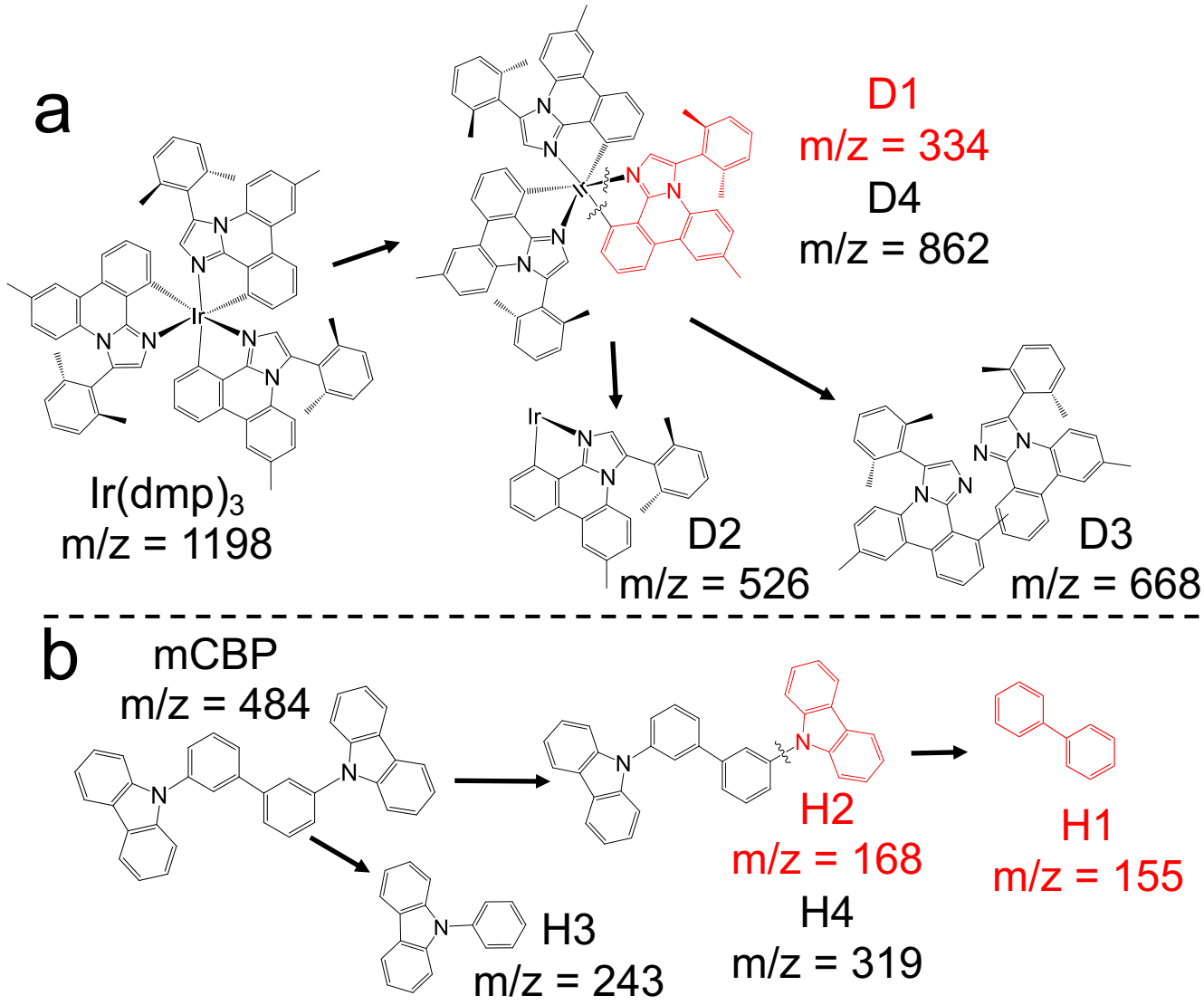
a
Ir(dmp)3
m/z = 1198
D1
m/z = 334
D4
m/z = 862
D2
m/z = 526
D3
m/z = 668
b
mCBP
m/z = 484
H3
m/z = 243
H2
m/z = 168
H4
m/z = 319
H1
m/z = 155

Figure 4

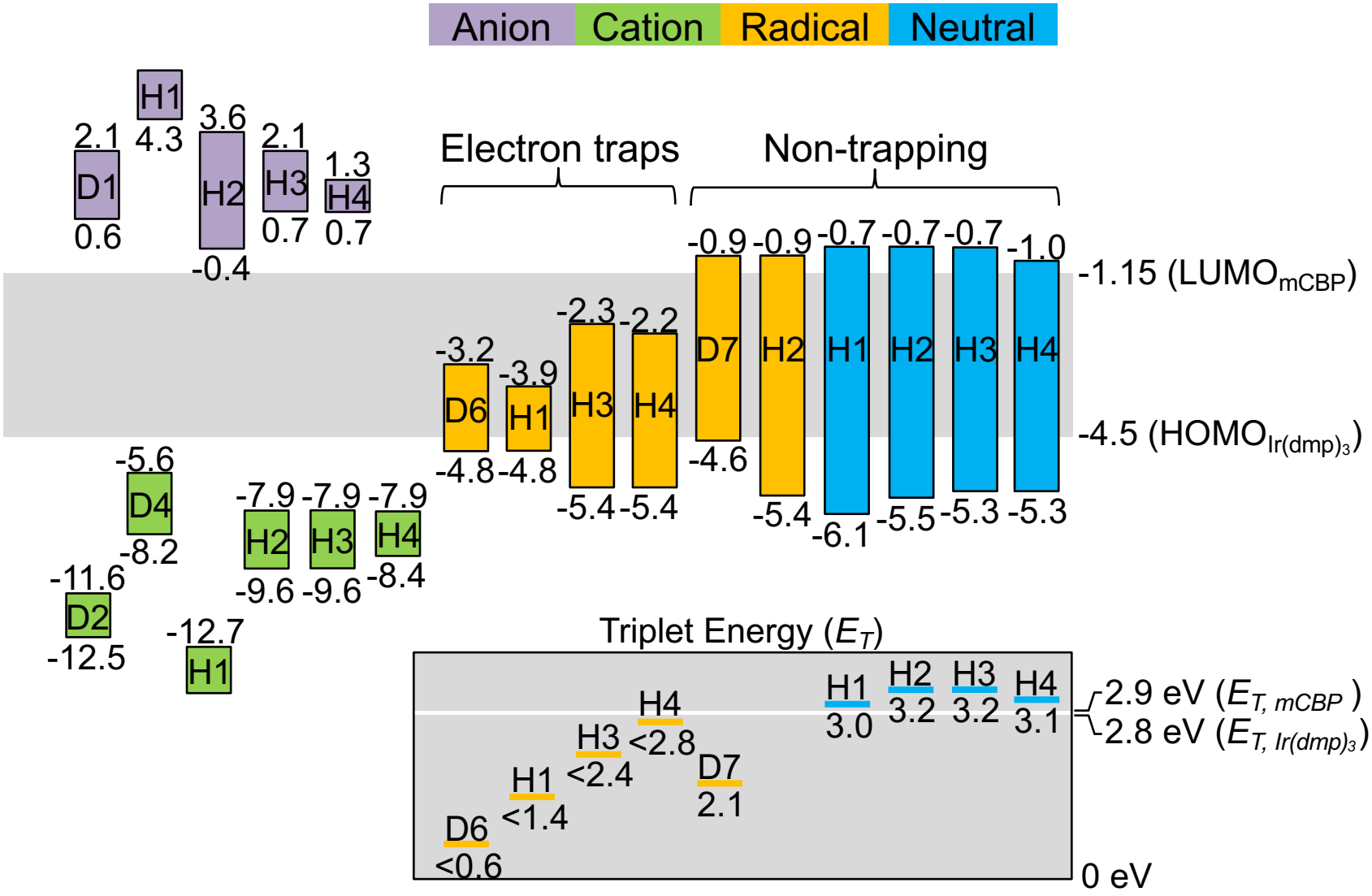
Anion
Cation
Radical
Neutral
Electron traps
Non-trapping
2.1
D1
0.6
4.3
H1
3.6
H2
-0.4
2.1
H3
0.7
1.3
H4
0.7
-3.2
D6
-4.8
-3.9
H1
-4.8
-2.3
H3
-5.4
-2.2
H4
-5.4
-0.9
D7
-4.6
-0.9
H2
-5.4
-0.7
H1
-6.1
-0.7
H2
-5.5
-0.7
H3
-5.3
-1.0
H4
-5.3
-1.15 (LUMO$_{mCBP}$)
-4.5 (HOMO$_{Ir(dmp)_3}$)
-5.6
D4
-8.2
-11.6
D2
-12.5
-12.7
H1
-7.9
H2
-9.6
-7.9
H3
-9.6
-7.9
H4
-8.4
Triplet Energy (E_T)
H4
H3 <2.8
H1 <2.4
D7
2.1
D6
<0.6
H1
3.0
H2
3.2
H3
3.2
H4
3.1
2.9 eV ($E_{T,\ mCBP}$)
2.8 eV ($E_{T,\ Ir(dmp)_3}$)
0 eV

Figure 5

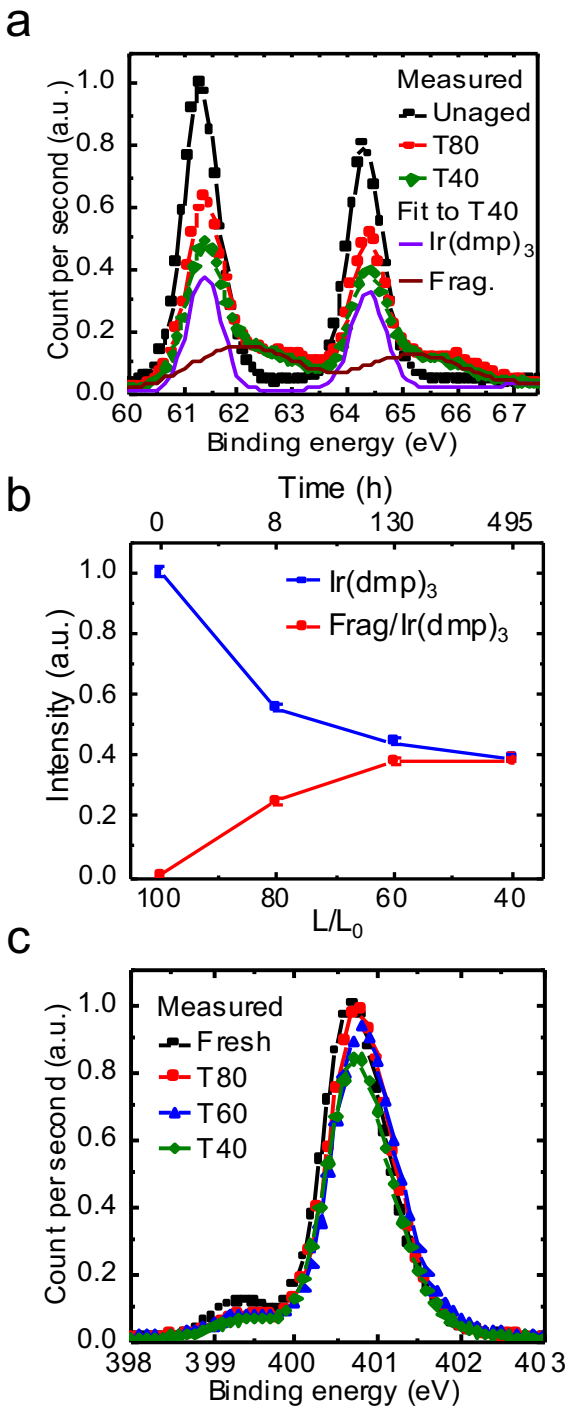
a
Measured
Unaged
T80
T40
Fit to T40
Ir(dmp)3
Frag.
Count per second (a.u.)
Binding energy (eV)
b
Time (h)
0
8
130
495
Ir(dmp)3
Frag/Ir(dmp)3
Intensity (a.u.)
L/L0
c
Measured
Fresh
T80
T60
T40
Count per second (a.u.)
Binding energy (eV)
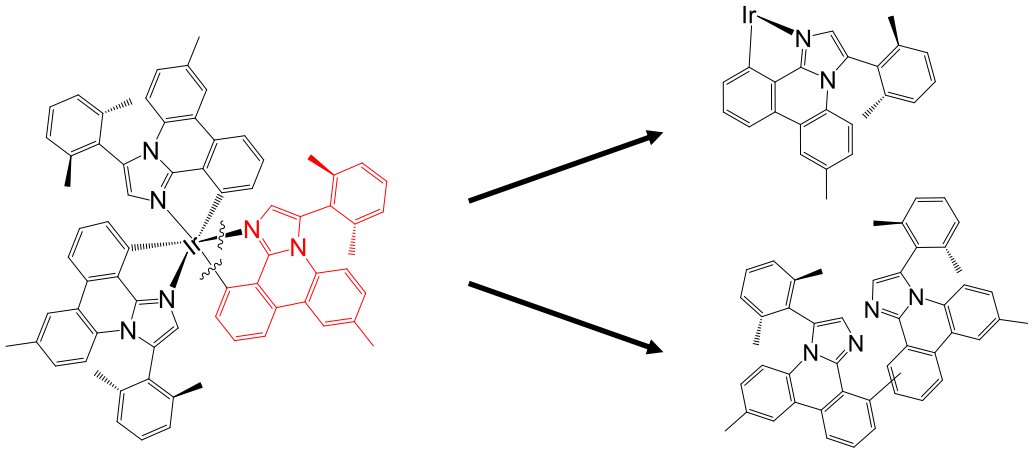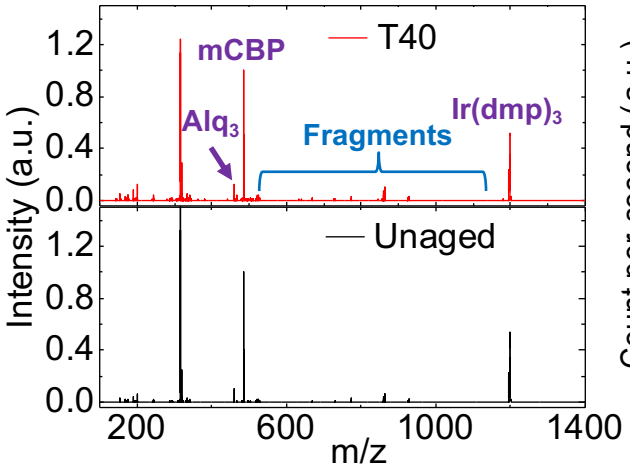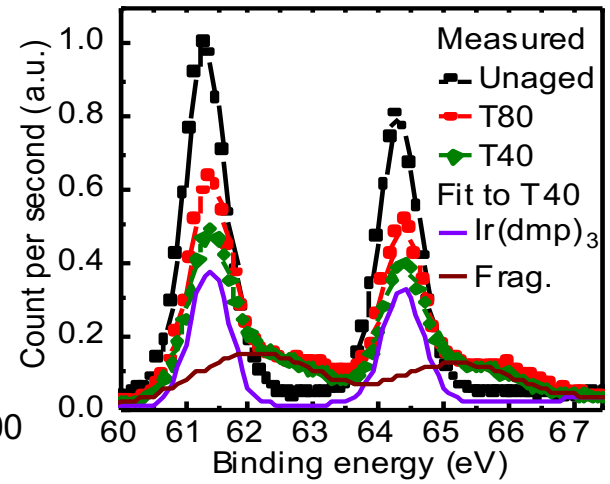
Graphical abstract